Nonequilibrium Spin Hall Accumulation in Ballistic Semiconductor Nanostructures

Branislav K. Nikolić,[1] Satofumi Souma,[1] Liviu P. Zârbo,[1] and Jairo Sinova[2]
[1]*Department of Physics and Astronomy, University of Delaware, Newark, Delaware 19716-2570, USA*
[2]*Department of Physics, Texas A&M University, College Station, Texas 77843-4242, USA*
(Received 21 December 2004; published 20 July 2005)

We demonstrate that the flow of a longitudinal unpolarized current through a *ballistic* two-dimensional electron gas with Rashba spin-orbit coupling will induce a nonequilibrium spin accumulation which has *opposite* signs for the two lateral edges and is, therefore, the principal observable signature of the spin Hall effect in two-probe semiconductor nanostructures. The magnitude of its out-of-plane component is gradually diminished by static disorder, while it can be enhanced by an in-plane transverse magnetic field. Moreover, our prediction of the longitudinal component of the spin Hall accumulation, which is insensitive to the reversal of the bias voltage, offers direct evidence to differentiate experimentally between the extrinsic, intrinsic, and mesoscopic spin Hall mechanisms.

DOI: 10.1103/PhysRevLett.95.046601 PACS numbers: 72.25.Dc, 85.75.Nn

Introduction.—When electric current flows along a conductor subjected to a perpendicular magnetic field, the Lorenz force deflects the charge carriers creating a transverse Hall voltage between the lateral edges of the sample. The normal Hall effect is one of the most familiar phenomena, as well as a widely utilized tool, in condensed matter physics [1]. In the absence of an external magnetic field, more esoteric Hall-type effects involving electron spin become possible in paramagnetic systems with spin-orbit (SO) couplings—the opposite spins can be separated and then accumulated on the lateral edges when they are transported by a *pure* (i.e., not accompanied by any net charge current) spin Hall current flowing in the transverse direction in response to unpolarized charge current in the longitudinal direction. For instance, the SO dependent scattering off impurities, which deflects spin-↑ and spin-↓ electrons of an unpolarized beam in opposite directions and is partially responsible for the anomalous Hall effect in ferromagnetic metals [1], has been invoked in early studies to predict the *extrinsic* (i.e., due to impurity scattering) spin Hall effect [2].

The pursuit of all-electrical spin current induction and manipulation in semiconductor spintronics [3] has rekindled interest in the realm of the spin Hall effect(s). In particular, recent theoretical arguments have unearthed the possibility for pure transverse spin Hall current that is several orders of magnitude greater than in the case of the extrinsic effect, arising due to *intrinsic* mechanisms related to the spin-split band structure in SO coupled bulk [4,5] or mesoscopic [6–8] semiconductor systems. While these theories are formulated in terms of not directly observable spin currents (which are the Fermi-sea quantity and not conserved in infinite homogeneous systems of the intrinsic effect [4,5], or the Fermi-surface property and conserved ones in the transverse electrodes attached to mesoscopic samples [6–8]), their detection requires one to measure nonequilibrium spin accumulation that they deposit at the sample edges [2,9,10]. The controversy in theoretical interpretations [11,12] of recent breakthrough observations of the spin Hall accumulation [9,10] is largely due to the fact that *no theory exists* that demonstrates the existence of such accumulation in *ballistic* SO coupled devices accessible to experiments.

To resolve these fundamental issues, in this Letter we formulate a Landauer-Keldysh approach [13,14] to the spin Hall accumulation problem in two-terminal devices, which treats phase-coherent spin-charge transport while taking into account all boundaries, interfaces, and electrodes of the semiconductor nanostructure [15]. We predict a non-

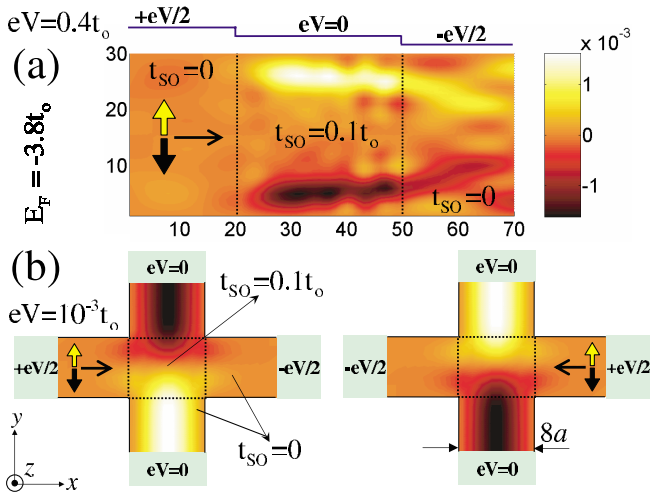

FIG. 1 (color online). (a) The out-of-plane component $\langle S_z(\mathbf{r})\rangle$ of the nonequilibrium spin accumulation induced by nonlinear quantum transport of unpolarized charge current injected from the left lead into a two-terminal *clean* 2DEG (of size $L = 30a > L_{\mathrm{SO}}$, $a \simeq 3$ nm) nanostructure with the Rashba SO coupling $t_{\mathrm{SO}} = 0.1t_o$ and spin precession length $L_{\mathrm{SO}} \approx 15.7a$. (b) Shows how lateral spin-↑ and spin-↓ densities will *flow* in opposite directions through the attached transverse ideal ($t_{\mathrm{SO}} = 0$) leads to generate a linear response spin Hall current $[I_y^s]^z$ out of four-terminal 2DEG ($L = 8a < L_{\mathrm{SO}}$) nanostructures [6], which changes sign $[I_y^s]^z(-V) = -[I_y^s]^z(V)$ upon reversing the bias voltage.

equilibrium spin accumulation induced at the lateral edges of a ballistic two-dimensional electron gas (2DEG) with Rashba SO coupling attached to two ideal (interaction-free) semi-infinite leads as a response to unpolarized charge current flowing through the sample, as shown in Fig. 1(a). The electric field along the z axis, which confines electrons within the xy plane of the quantum well in semiconductor heterostructure, generates an effective momentum-dependent magnetic field $\mathbf{B}_{\mathrm{R}}(\mathbf{p})$ [which does not break time-reversal invariance] due to the Rashba SO coupling [3,16]. The pattern of local spin density throughout the device is obtained from

$$\langle \mathbf{S}(\mathbf{r}) \rangle = \frac{\hbar}{2} \int_{E_F - eV/2}^{E_F + eV/2} \frac{dE}{2\pi i} \, \mathrm{Tr}_{\mathrm{spin}}[\hat{\boldsymbol{\sigma}} \mathbf{G}^{<}(\mathbf{r}, \mathbf{r}; E, V)], \quad (1)$$

where the exact spin-dependent lesser nonequilibrium Green function $\mathbf{G}^{<}(\mathbf{r}, \mathbf{r}'; E, V)$ [13] is evaluated in the *steady-state* quantum transport through the semiconductor nanostructure attached to external probes [14]. Here V is the applied bias voltage between the leads and $\frac{\hbar}{2}\hat{\boldsymbol{\sigma}}$ is the spin-$\frac{1}{2}$ operator. In the nonlinear phase-coherent transport regime, Figs. 1(a) and 2 demonstrate that the transverse profile of the out-of-plane $\langle S_z(\mathbf{r}) \rangle$ component of the spin accumulation develops two peaks of opposite signs at the lateral edges of the 2DEG. Upon reversing the bias voltage, the edge peaks flip their sign $\langle S_z(\mathbf{r}) \rangle_{-V} = -\langle S_z(\mathbf{r}) \rangle_V$. Around the left-lead–2DEG interface, $\langle S_z(\mathbf{r}) \rangle \to 0$ in Fig. 1(a) is suppressed since unpolarized electrons are injected at this contact.

All three features of $\langle S_z(\mathbf{r}) \rangle$, delineated here for the phase-coherent transport regime at low temperatures, are remarkably similar to the general phenomenology of the spin Hall effect which has been demonstrated convincingly in two very recent experiments [9,10]. These experiments focus on the optical detection of the spin Hall accumulation of opposite signs on the lateral edges of two-probe semiconductor structures (in the semiclassical transport regime at finite temperatures): (i) weakly SO coupled 3D films of GaAs or strained InGaAs [9], and (ii) strongly SO coupled 2D hole gases [10]. The former experiment has been interpreted as the manifestation of the extrinsic effect [2,11] due to the small resulting polarization ($\sim 0.03\%$) and no SO splitting of the band structure [9], while the latter is consistent with the intrinsic mechanisms [5,12] because of spin-split quasiparticle energies and much larger spin polarization ($\sim 1\%$) [10].

However, it has been estimated that spin Hall accumulation induced by the extrinsic effect is far below present experimental sensitivity [12]. On the other hand, it has been argued [11,16] that the intrinsic spin Hall current in the bulk, determined only by the equilibrium distribution function and spin-split Bloch band structure [4,5], does not really transport spins, so that no spin accumulation at the edges is possible in the absence of impurities [11]. We bring such debates to an end in Fig. 1(b) by attaching two additional transverse ideal semi-infinite leads at the lateral edges of a perfectly clean 2DEG and showing how spin-$\uparrow$ and spin-$\downarrow$ densities will *flow* through those leads in *opposite* transverse directions to generate the spin Hall current driven by mechanisms [17] on the *mesoscopic* scale [18] set by the spin precession length [6]. Thus, Fig. 1(b) demonstrates convincingly that spin Hall effect in SO coupled ballistic nanostructures can be used as an all-electrical semiconductor-based spin injector [3].

The attempts [19,20] to understand the spin Hall accumulation in macroscopic *disordered* Rashba spin-split 2DEG attached to two massive electrodes have reached contradictory conclusions (vanishing $\langle S_z(\mathbf{r}) \rangle$ on the lateral edges [19] vs $\langle S_z(\mathbf{r}) \rangle \neq 0$ at the edges and within the sample [20]), which can be traced to an incomplete treatment of experimentally relevant measuring geometry within the semiclassical diffusion equation approaches. A plethora of spin transport phenomena illustrate the need to treat the whole device geometry due to the presence of SO couplings, even in the semiclassical transport regime [18]. For example, spin relaxation in confined Rashba structures is quite different from the bulk spin relaxation of D'yakonov and Perel' (DP) [3] because of the transverse confinement effects [21] or chaotic vs integrable boundary scattering [22]. Also, $\mathbf{B}_{\mathrm{R}}(\mathbf{p})$ in Rashba SO coupled wires is almost parallel to the transverse direction [17] (in contrast to the infinite 2DEG where no unique spin quantization axis exists [5]). Mesoscopic transport techniques, developed to treat the whole measuring geometry as demanded by quantum coherence effects [15], are well suited to handle all relevant details of the spin Hall transport measurement setups [9,10]. Therefore, we apply [14] the Keldysh Green functions [13] to the Landauer-type geometry [15] where the finite-size sample is attached to two macroscopic reservoirs via semi-infinite ideal leads (which simplify the boundary conditions)—here the current is limited by quantum transmission through a potential profile while power is dissipated nonlocally in the reservoirs [14,15].

Landauer-Keldysh Green function approach to nonequilibrium spin accumulation.—The effective mass Hamiltonian modeling the ballistic finite-size 2DEG with Rashba SO coupling in Fig. 1 is given by [3,16]

$$\hat{H} = \frac{\hat{p}_x^2 + \hat{p}_y^2}{2m^*} + \frac{\alpha}{\hbar}(\hat{p}_y \hat{\sigma}_x - \hat{p}_x \hat{\sigma}_y) + V_{\mathrm{conf}}(x, y), \quad (2)$$

where $(\hat{\sigma}_x, \hat{\sigma}_y, \hat{\sigma}_z)$ is the vector of the Pauli matrices, $(\hat{p}_x, \hat{p}_y)$ is the momentum operator in 2D space, α is the strength of the Rashba SO coupling [16], and $V_{\mathrm{conf}}(x, y)$ is the transverse confining potential. In order to evaluate the nonequilibrium Green functions for a sample of arbitrary shape attached to the ideal leads, we follow Ref. [14] and employ the local orbital basis. In this representation, the Rashba Hamiltonian is expressed as [21]

$$\hat{H} = \sum_{\mathbf{m}\sigma} \varepsilon_{\mathbf{m}} \hat{c}^{\dagger}_{\mathbf{m}\sigma} \hat{c}_{\mathbf{m}\sigma} + \sum_{\mathbf{m}\mathbf{m}'\sigma\sigma'} \hat{c}^{\dagger}_{\mathbf{m}\sigma} t^{\sigma\sigma'}_{\mathbf{m}\mathbf{m}'} \hat{c}_{\mathbf{m}'\sigma'}, \quad (3)$$

where hard wall boundary conditions account for confinement on the $L \times L$ lattice with lattice spacing a (typically $a \simeq 3$ nm [21]). Here $\hat{c}^{\dagger}_{\mathbf{m}\sigma}$ ($\hat{c}_{\mathbf{m}\sigma}$) is the creation (annihilation) operator of an electron at the site $\mathbf{m} = (m_x, m_y)$. The generalized nearest neighbor hopping $t^{\sigma\sigma'}_{\mathbf{mm}'} = (\mathbf{t}_{\mathbf{mm}'})_{\sigma\sigma'}$ accounts for the Rashba coupling

$$\mathbf{t}_{\mathbf{mm}'} = \begin{cases} -t_o I_s - i t_{SO}\hat{\sigma}_y & (\mathbf{m} = \mathbf{m}' + \mathbf{e}_x), \\ -t_o I_s + i t_{SO}\hat{\sigma}_x & (\mathbf{m} = \mathbf{m}' + \mathbf{e}_y), \end{cases} \quad (4)$$

through the SO hopping parameter $t_{SO} = \alpha/2a$ (I_s is the unit 2×2 matrix in the spin space). The direct correspondence between the continuous Eq. (2) and the lattice Hamiltonian Eq. (3) is established by using $t_o = \hbar^2/2m^*a^2$ for the orbital hopping and by selecting the Fermi energy $E_F = -3.8t_o$ close to the bottom of the band at $-4.0t_o$ to ensure the parabolic energy-momentum dispersion.

At time $t' = -\infty$ the 2DEG and the leads are not connected, while the left and the right leads are in their own thermal equilibrium with the chemical potentials μ_L and μ_R, respectively, where $\mu_L = \mu_R + eV$. The adiabatic switching of the hopping parameter connecting the leads and the 2DEG generates time evolution of the density matrix of the structure [14]. The spin accumulation is obtained as the nonequilibrium statistical average $\langle \cdots \rangle$ (with respect to the density matrix at $t' = 0$ [13]) of the spin-density operator $\langle \hat{\mathbf{S}}_{\mathbf{m}} \rangle = \frac{\hbar}{2}\sum_{\sigma\sigma'} \boldsymbol{\sigma}_{\sigma\sigma'} \langle \hat{c}^{\dagger}_{\mathbf{m}\sigma}\hat{c}_{\mathbf{m}\sigma'} \rangle$, which is expressed via the lesser Green function $\langle \hat{c}^{\dagger}_{\mathbf{m}\sigma}\hat{c}_{\mathbf{m}'\sigma'} \rangle = \frac{\hbar}{i} G^{<}_{\mathbf{m}'\mathbf{m},\sigma'\sigma}(\tau = 0) = \frac{1}{2\pi i}\int_{-\infty}^{\infty} dE G^{<}_{\mathbf{m}'\mathbf{m},\sigma'\sigma}(E)$, thereby yielding Eq. (1). The matrix $\mathbf{G}^{<}(E)$ is obtained from the Keldysh equation $\mathbf{G}^{<}(E) = \mathbf{G}^{r}(E)\boldsymbol{\Sigma}^{<}(E)\mathbf{G}^{a}(E)$. This equation can be solved exactly in the noninteracting electron approximation by evaluating the retarded $\mathbf{G}^{r}(E) = [E - \mathbf{H} - U_{\mathbf{m}} - \boldsymbol{\Sigma}^{r}_{L} - \boldsymbol{\Sigma}^{r}_{R}]^{-1}$ and the advanced $\mathbf{G}^{a}(E) = [\mathbf{G}^{r}(E)]^{\dagger}$ Green function matrices, where the self-energies $\boldsymbol{\Sigma}^{r}_{L}(E - eV/2)$, $\boldsymbol{\Sigma}^{r}_{R}(E + eV/2)$, and $\boldsymbol{\Sigma}^{<}(E) = -2i[\mathrm{Im}\boldsymbol{\Sigma}_{L}(E - eV/2)f_{L}(E - eV/2) + \mathrm{Im}\boldsymbol{\Sigma}_{R}(E + eV/2) \times f_{R}(E + eV/2)]$ (in the absence of inelastic processes) are introduced by the interaction with the leads [14]—their dependence on V, together with the electric potential landscape $U_{\mathbf{m}}$ within the sample in $\mathbf{G}^{r}(E)$, ensures the gauge invariance of measurable quantities.

Nonequilibrium spin accumulation in clean mesoscopic two-probe 2DEG structures.—The one-dimensional spatial transverse profile [9] of $\langle \mathbf{S}(x = x_0, y) \rangle$ across the macroscopic ($200a \times 200a$) 2DEG sample supporting steady-state charge current at zero temperature is plotted in Fig. 2 for the *nonlinear* $eV \sim E_F$ as well as the *linear* $eV \ll E_F$ transport regime. In the linear phase-coherent transport regime at low temperatures only states at the Fermi energy contribute to $\langle \mathbf{S}(\mathbf{r}) \rangle$ in Eq. (1), which therefore encodes the information about their wave function and oscillates within the sample. Figure 2 also shows that the width of the edge peaks of $\langle S_z(\mathbf{r}) \rangle$ is determined by the spin precession length $L_{SO} = \pi a t_o/2t_{SO}$ [21] (on which spin precesses by an angle π; L_{SO} also plays the role of the DP spin relaxation length [3,22] in weakly disordered systems) in our two-probe device which is in the regime $L > L_{SO} \gg \lambda_F$.

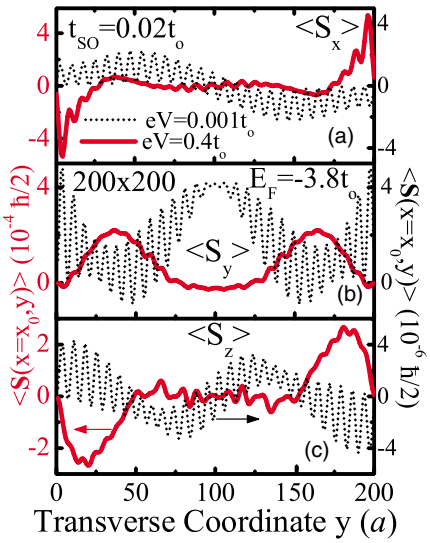

FIG. 2 (color online). The one-dimensional transverse spatial profile of the spin accumulation $\langle \mathbf{S}(x = 78a, y) \rangle$ across the $200a \times 200a$ 2DEG with the Rashba SO coupling $t_{SO} = 0.02t_o$ through which *ballistic* quantum transport takes place in the nonlinear regime $eV = 0.4t_o$ (solid lines) or the linear regime $eV = 10^{-3}t_o$ (dotted lines). The width of the edge peaks of $\langle S_z(x = 78a, y) \rangle$ is $\approx L_{SO}/2 = \pi a t_o/4t_{SO}$.

While experiments [9,10] have searched for the out-of-plane spin accumulation exhibiting opposite signs on the lateral edges as evidence for the spin Hall effect, we predict that *both* $\langle S_z(\mathbf{r}) \rangle$ and $\langle S_x(\mathbf{r}) \rangle$ satisfy this criterion. The emergence of $\langle S_x(\mathbf{r}) \rangle \neq 0$ is the hallmark of the mesoscopic spin Hall effect [6] in Rashba wires where Hamiltonian Eq. (2) gives rise to the SO force operator [17] $\hat{\mathbf{F}} = 2\alpha^2 m^* (\hat{\mathbf{p}} \times \mathbf{z}) \otimes \hat{\sigma}_z/\hbar^3 - dV_{\mathrm{conf}}(\hat{y})\mathbf{y}/d\hat{y}$ which deflects spin-$\uparrow$ and spin-$\downarrow$ electronic wave packets in opposite transverse directions, while spin is at the same time precessing since injected $|\uparrow\rangle$, $|\downarrow\rangle$ (the eigenstates of $\hat{\sigma}_z$) are not the eigenstates of the Zeeman term $\hat{\boldsymbol{\sigma}} \cdot \mathbf{B}_{\mathrm{R}}(\mathbf{p})$ whose $\mathbf{B}_{\mathrm{R}}(\mathbf{p})$ field is almost parallel to the y axis [17,21]. This semiclassical picture [17] heuristically explains the symmetry properties of the quantum transport induced accumulations in Fig. 2 with respect to the bias voltage reversal, $\langle S_z(\mathbf{r}) \rangle_{-V} = -\langle S_z(\mathbf{r}) \rangle_{V}$ vs $\langle S_x(\mathbf{r}) \rangle_{-V} = \langle S_x(\mathbf{r}) \rangle_{V}$, which can be tested experimentally [10]. Also, the α^2-dependent transverse SO "force" accounts for the difference $\langle S_z(\mathbf{r}) \rangle_{-\alpha} = \langle S_z(\mathbf{r}) \rangle_{\alpha}$ vs $\langle S_x(\mathbf{r}) \rangle_{-\alpha} = -\langle S_x(\mathbf{r}) \rangle_{\alpha}$. Finally, Fig. 2(a) confirms that $\langle S_z(\mathbf{r}) \rangle$ spin densities will move away from the lateral edges upon entering the right lead where $\alpha \equiv 0$ and the transverse SO force deflecting the spins is absent.

In contrast to the out-of-plane $\langle S_z(\mathbf{r}) \rangle$ and the in-plane longitudinal $\langle S_x(\mathbf{r}) \rangle$ spin Hall accumulations, the transverse in-plane spin accumulation $\langle S_y(\mathbf{r}) \rangle$ has the same sign on both lateral edges. Thus, it cannot originate from

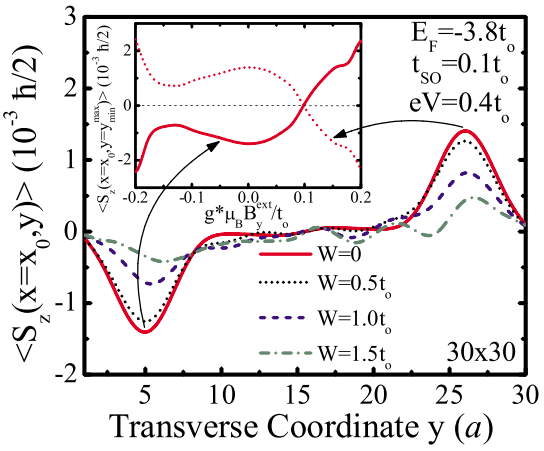

FIG. 3 (color online). The transverse profile $\langle S_z(x = 13a, y)\rangle$ of spin Hall accumulation as a function of spin-independent disorder W setting the mean free path $\ell \approx 21.5a/W^2$ [the ballistic limit $W = 0$ is the transverse profile of $\langle S_z(\mathbf{r})\rangle$ in Fig. 1(a)]. The inset shows the effect of the external in-plane magnetic field $g^*\mu_B B_y^{\rm ext}$ on $\langle S_z(x = 13a, y = y_{\rm min}^{\rm max})\rangle$ at its maximum $y^{\rm max} = 26a$ or minimum $y_{\rm min} = 5a$ peak values.

the spin Hall effect. Instead, it is an analog of the magnetoelectric effect—where the electric field induces spin polarization of conduction electrons and nonequilibrium magnetization $\mathbf{M} = \beta\mathbf{E}$—which was argued to occur in *disordered* paramagnetic systems (metals with SO scattering off impurities [23] or diffusive Rashba spin-split 2DEG [19,24]), and has finally been observed experimentally [25]. It arises due to the combined effect of SO coupling, inversion asymmetry, and time-reversal symmetry breaking by electron scattering (which is necessary due to $\mathbf{M}$ being t odd while $\mathbf{E}$ is t even). However, here we predict that the passage of electric current through the *ballistic* sample ($\mathbf{E} = 0$ inside 2DEG) will also induce the transverse in-plane magnetization, where the finite quantum point contact conductance of the nanostructure in Fig. 1(a) (i.e., the corresponding dissipation in the reservoirs [14,15]) signifies the time-reversal symmetry breaking.

The key issue for spintronics applications is to detect (at least indirectly [2,8]) the pure spin Hall current flowing out of multiterminal structures. When transverse leads (e.g., labeled by 2 and 3) are attached to the lateral edges of 2DEG, the nonequilibrium spin accumulation will push the pure spin current $\frac{\hbar}{2e}(I_2^{\uparrow} - I_2^{\downarrow})$ into them, as shown in Fig. 1(b). The properties of its spin Hall $[I_2^s]^z = -[I_3^s]^z$, $[I_2^s]^x = -[I_3^s]^x$, and spin "polarization" $[I_2^s]^y = [I_3^s]^y$ components predicted in Ref. [6] are exactly the same as can be inferred from the profiles of $\langle\mathbf{S}(\mathbf{r})\rangle$ in Fig. 2.

The effect of disorder and in-plane magnetic field on the mesoscopic spin Hall accumulation.—We show in Fig. 3 that disorder, introduced as the random potential $\varepsilon_{\mathbf{m}} \in [-W/2, W/2]$ in Eq. (3), is gradually diminishing the amplitude of the original clean limit edge peaks of $\langle S_z(\mathbf{r})\rangle$ while leaving their position intact. Thus, the magnitude of the peaks alone does not provide a single criterion to differentiate between possible underlying mechanisms of the spin Hall effects [9,12]. We offer here yet another experimental tool (in addition to the $\langle S_x(\mathbf{r})\rangle_{-V} = \langle S_x(\mathbf{r})\rangle_V$ test) to identify the mesoscopic spin Hall mechanism by demonstrating in the inset of Fig. 3 that an external in-plane transverse magnetic field $B_y^{\rm ext}$, which in strictly 2D systems does not affect orbital degrees of freedom, will not destroy the edge peaks of $\langle S_z(\mathbf{r})\rangle$, except when the Rashba field $\mathbf{B}_{\rm R}(\mathbf{p})$ term is canceled by the Zeeman spin splitting term $g^*\mu_B B_y^{\rm ext}$.

We are grateful to E. I. Rashba, L. Sheng, A. H. MacDonald, and T. Jungwirth for valuable discussions. This research was supported in part by ACS Grant No. PRF-41331-G10.

[1] *The Hall Effect and its Applications*, edited by C. L. Chien and C. W. Westgate (Plenum, New York, 1980).
[2] M. I. D'yakonov and V. I. Perel', JETP Lett. **13**, 467 (1971); J. E. Hirsch, Phys. Rev. Lett. **83**, 1834 (1999).
[3] I. Žutić, J. Fabian, and S. Das Sarma, Rev. Mod. Phys. **76**, 323 (2004).
[4] S. Murakami, N. Nagaosa, and S.-C. Zhang, Science **301**, 1348 (2003); Phys. Rev. B **69**, 235206 (2004).
[5] J. Sinova *et al.*, Phys. Rev. Lett. **92**, 126603 (2004).
[6] B. K. Nikolić, L. P. Zârbo, and S. Souma, cond-mat/0408693 [Phys. Rev. B (to be published)].
[7] L. Sheng, D. N. Sheng, and C. S. Ting, Phys. Rev. Lett. **94**, 016602 (2005).
[8] E. M. Hankiewicz *et al.*, Phys. Rev. B **70**, 241301(R) (2004).
[9] Y. K. Kato *et al.*, Science **306**, 1910 (2004).
[10] J. Wunderlich *et al.*, Phys. Rev. Lett. **94**, 047204 (2005).
[11] S. Zhang and Z. Yang, Phys. Rev. Lett. **94**, 066602 (2005).
[12] B. A. Bernevig and S.-C. Zhang, cond-mat/0412550.
[13] L. V. Keldysh, Sov. Phys. JETP **20**, 1018 (1965).
[14] C. Caroli *et al.*, J. Phys. C **4**, 916 (1971).
[15] H. U. Baranger and A. D. Stone, Phys. Rev. B **40**, 8169 (1989).
[16] E. I. Rashba, Phys. Rev. B **70**, 161201(R) (2004).
[17] B. K. Nikolić, L. P. Zârbo, and S. Welack, cond-mat/0503415 [Phys. Rev. B (to be published)].
[18] M. Zaffalon and B. J. van Wees, Phys. Rev. B **71**, 125401 (2005).
[19] E. G. Mishchenko, A. V. Shytov, and B. I. Halperin, Phys. Rev. Lett. **93**, 226602 (2004).
[20] X. Ma *et al.*, Phys. Rev. B **70**, 195343 (2004).
[21] B. K. Nikolić and S. Souma, Phys. Rev. B **71**, 195328 (2005).
[22] C.-H. Chang, A. G. Mal'shukov, and K. A. Chao, Phys. Rev. B **70**, 245309 (2004); O. Zaitsev, D. Frustaglia, and K. Richter, Phys. Rev. Lett. **94**, 026809 (2005).
[23] L. S. Levitov, Yu. V. Nazarov, and G. M. Eliashberg, Sov. Phys. JETP **61**, 133 (1985).
[24] V. M. Edelstein, Solid State Commun. **73**, 233 (1990); J. I. Inoue, G. E. W. Bauer, and L. W. Molenkamp, Phys. Rev. B **67**, 033104 (2003).
[25] S. D. Ganichev *et al.*, cond-mat/0403641.